Biaxial Fatigue Testing and Simulation of Cruciform Sub-Structure

Bender, Jens Jakob; Lindgaard, Esben; Overgaard, Lars Christian

DOI (link to publication from Publisher):
10.5278/vbn.287100540

Publication date:
2018

Document Version
Other version

Biaxial Fatigue Testing and Simulation of Cruciform Sub-Structure

Jens Jakob Bender, Esben Lindgaard and Lars Christian Terndrup Overgaard
Department of Materials and Production, Aalborg University,
Fibigerstraede 16, 9220 Aalborg East, Denmark

Abstract

In this work, numerical simulations and experimental tests are performed to determine if it is possible to accurately predict the fatigue behaviour of a glass fibre reinforced polymer (GFRP) sub-structure, when fatigue data from a fatigue material database is used in combination with static properties of the actual material. Firstly an appropriate sub-structure is designed based on biaxial test specimens readily found in the literature. The main objective during the design phase is to produce a sub-structure where inter-fibre failure occurs in a typical wind turbine blade laminate when a prescribed biaxial constant amplitude load is applied. The designed sub-structure is tested in biaxial fatigue, and it is shown that there is no delamination in the ply-drops in the gauge zone and that first failure occurs in the gauge zone without cracks from the corners propagating into the gauge zone. This is achieved by using internal ply-drops and a cross-ply dominated lay-up. Lastly, a simulation of the fatigue test is conducted where the linear progressive strength degradation model FADAS (Fatigue Damage Simulator) algorithm is applied. The algorithm is applied to predict the progressive damage in the corners, because this influences the stress and strain field in the gauge zone.

Keywords: *Glass fibres, Life prediction, Matrix cracking, Internal ply-drops, Fatigue*

1. Introduction

Glass Fibre Reinforced Polymers (GFRP) are becoming widespread in many industries because of their high stiffness and strength to weight ratio. In the wind turbine industry, GFRP has been used for decades, but there are still many challenges in predicting the stiffness and strength degradation through the fatigue life, especially when taking multiaxial loading into account. The reason for the difficulty in predicting the fatigue life is two fold. The first reason is that the usual applied test methods are either very expensive (full scale testing) or not representable of a wind turbine blade (coupon test), and the other is that the fatigue life prediction models are too inaccurate. These issues are considered in the following.

Since full scale tests are expensive, and coupon tests do not resemble wind turbine blades, it seems logical to perform tests and simulations on sub-structures. The biggest issue with sub-structures is the design. There are no standards for sub-structures, and it is difficult to design it in such a way that the applied loads produce the same far-field stresses and strains as in the blade. A sub-structure can resemble a structural detail in a wind turbine blade, and is far less expensive than a full scale test. A sub-structure can be designed in many ways depending on what is to be tested, and what kind of output is desired. Inspiration for the design of the sub-structure in this work is obtained among test specimens that are used for biaxial testing. In this work, a sub-structure is considered instead of a coupon specimen to avoid the short-comings stated above. However, this leads to manufacturing difficulties in getting a perfect test specimen and failure modes inside the gauge zone.

In general, three different types of test specimen for biaxial testing exist; tubular specimens, off-axis specimens and cruciform specimens. As mentioned, the off-axis coupon test specimens can not resemble a wind turbine blade, primarily due to free-edge-effects. Therefore, these are not considered further.

The tubular specimens have been tested extensively in the literature [1–5]. The primary advantage is that the laminate can be tested without influence of free-edge effects. However, the manufacturing process is quite complex [6] and premature failure can arise at the transitions from the clamping area to the test area, and at the overlap in the longitudinal direction if the filament winding technique is not used. Any in-plane load condition can be tested, but only for thin laminates.

The cruciform test specimen allows for a large variety of lay-ups to be tested, and it is possible to apply any in-plane stress state, as long as the inherent anisotropy of the GFRP is used to produce shear stresses. The biggest issue with cruciform specimens is that premature and unwanted failure may initiate in the corners between two adjacent arms or as premature delamination in ply-drops at the gauge zone and not in the gauge zone of the specimen as intended. These issues are detected and attempted solved in [7–13].

In the literature, fatigue life prediction models are divided into three classes. These are listed with increasing complexity and accuracy: fatigue life models, phenomenological models and mechanistic models [14].

Simple fatigue life models are used in the wind turbine industry, where no distinction is made between different failure modes, so in order to increase the accuracy of fatigue life predictions a more advanced approach is needed. Today the mechanistic models are still immature, which is why a phenomenological model is chosen in this work. The linear progressive Fatigue Damage Simulator (FADAS) is applied because it is state-of-the-art and readily available from the literature, where high accuracy has been demonstrated [15]. The FADAS model distinguishes between different failure modes on ply level, whereas mechanistic models operate with failure modes on a microscopic level, which therefore, makes the FADAS model a mix between phenomenological and mechanistic models.

FADAS requires input in the form of material stiffness and strength together with S-N data, which means that mechanical testing of unidirectional (UD) laminated test specimens is a prerequisite for applying the FADAS model. When applying current techniques these tests take several months to complete when testing non-stop on a single test machine. Therefore, it would be of great value to the industry if it was sufficient to test the static behaviour of the GFRP. The fatigue behaviour could then accurately be estimated based on fatigue tests of a similar GFRP.

There is generally large scatter on the average and variation of static properties of similar epoxy systems. However, the slope of the fatigue data is much more comparable for similar epoxy systems. Combined with the fact that fatigue strength variance scales with number of cycles due to the way damages develop in dissimilar initial imperfections, there is only reason to suspect that fatigue properties would be much more similar than static values for two GFRPs manufactured using the same fabric architectures and constituent types. From this consideration and the fact that the fatigue testing of coupon specimens is very time-consuming, it is of interest to test if the fatigue failure behaviour of a sub-structure can be accurately estimated when fatigue material data is obtained from a database, and static material data is obtained from the actual material. In this work,

first failure in the gauge zone is of interest, thus FADAS is used to simulate the progressive damage in the sub-structure, to account for damages outside of the gauge zone, which change the load path, and hereby the stress and strain field leading to first ply failure in the gauge zone.

2. Sub-structure Design

In this work, a specific lay-up and a multiaxial load condition is tested, both of these can be found in a wind turbine blade. The transitional part of the blade between the root and the aerofoil called the inboard part of the blade is one of the areas that experiences the highest levels of multiaxial loading. The load in this area comes from the flap-wise bending of the blade, which causes longitudinal strains, and the ovalisation of the cross section due to the lack of a stabilising shear web, which causes circumferential strains. A strain ratio of $\lambda = 0.34$ is chosen between strain in the circumferential and longitudinal direction to replicate the load condition. Moreover, the laminate in this part of the blade is very thick, which means that even though the thickness of the laminate is downscaled for the sub-structure, a rather thick laminate is required to be representative of the stress field in the actual blade.

Therefore, it is chosen to use a 3.3 mm laminate of $[\pm 45_2, 0_3]_{SO}$ where $_{SO}$ indicates that the lay-up is symmetric with an odd number of layers, equivalent to $[\pm 45_2, 0_5, \pm 45_2]$. The relatively thick lay-up would make it difficult to manufacture and test a sub-structure that resembles a tubular specimen. For this reason, in this work, it is chosen to design a sub-structure that resembles a cruciform specimen.
The cruciform sub-structure designed in this work is based on the geometry from two cruciform specimen designs, namely Laustsen et al. [16], where the general outer geometry is adapted from and Lamkanfi et al. [11], where the corners between the arms are used to reduce the load transfer between adjacent arms.
Delamination is unavoidable at the thickness tapering area in the specimen from [11] when milling is employed to decrease the thickness of the gauge zone of the cruciform test specimens [17]. These delaminations are due to the 3D effects arising at ply-drops. Internal ply-drops are applied in this work to decrease the risk of delamination in the ply-drops. The plies have to be cut by hand to create the gauge zone, and therefore, the gauge zone has straight edges to ease this process. The sub-structure is designed to be flat to simplify the manufacturing process and decrease the risk of manufacturing defects. A quarter model of the designed sub-structure is shown in Fig. 1.
The final geometry and lay-up of the sub-structure is determined through an automated numerical study using MATLAB 2014a software and the Finite Element program ANSYS v14.5, where the lay-up of the gauge zone is fixed by the industrial partner. The lay-up, thickness and corner geometry of the structure outside the gauge zone is determined through the numerical study to ensure that the load introduction areas do not fail during testing.
The sequence of the lay-up is shown in Fig. 1. The lay-up notations, except the one for the gauge zone, indicate the lay-up before the ply-drops are initiated, i.e. the lay-up notation indicates the lay-up for the thickest part of the section. From the outer to the inner boundary of a section the plies are dropped one by one, and at the inner boundary the lay-up is similar to the lay-up of the next section. The sub-structure is dominated by $[0, 90]$ plies in an attempt to decrease the shear strain in the corners. Moreover, it is chosen to drop the additional $[0]$ plies closest to the gauge zone because the fibres in the $[0]$ plies are parallel to the expected Inter Fibre Failure (IFF) fracture surfaces, which minimises the 3D effects. Hereby less disturbance and a more uniform strain field can be obtained close to the gauge

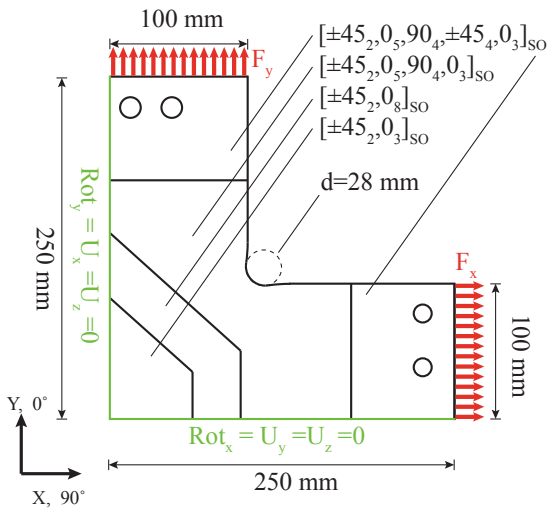

Fig. 1 Geometry, lay-up and FE boundary conditions of the designed sub-structure (quarter model)

zone. The $[\pm 45]$ plies are applied in the clamping areas to reduce the risk of tearout of the bolts.
The sub-structure is designed to be symmetric w.r.t. the centre-plane of the thickness which means that during the manufacturing, the sub-structure is put in a mould where the middle part (gauge and ply-drop zone) is elevated accordingly to ensure that the thickness of the gauge zone is tapered from both sides. The sub-structure is manufactured using the Vacuum Assisted Resin Transfer Moulding (VARTM) process where resin is transferred from one side of the sub-structure to the other by a vacuum.

2.1 Material Data

In this work, fatigue data from the OptiDAT research database [18] is used because this data was used to verify the applicability of the FADAS algorithm [15]. Specifically, the material is a GFRP consisting of the epoxy system "PRIME 20" with glass fibre reinforcements "PPG 2002" as described in [19]. The fibre volume fraction is specified to 55 ± 3% for the [0] and [90] laminates, and for the $[\pm 45]$ it is 52 ± 3% and the corresponding material properties are shown in Table 1. The static material properties used in this work are obtained from the material used in the manufacturing of the sub-structures. The actual values are withheld due to a confidentiality agreement. The implemented linear FADAS algorithm has been verified by simulating a fatigue test on the R03 coupon test specimen defined in the OptiDAT wind turbine materials research database [18]. The results are more or less similar to the results in [20].

$\sigma_a = \sigma_0 N^{(-\frac{1}{k})}$

	R=0.1		R=-1		R=10	
	σ_0 [MPa]	k [-]	σ_0 [MPa]	k [-]	σ_0 [MPa]	k [-]
σ_1	500.8	10.03	972.2	8.05	289.5	26.08
σ_2	50.2	8.63	87.5	8.43	88.5	24.32
σ_6	38.1	11.06	N/A	N/A	N/A	N/A

Table 1 Fatigue material data for the OptiDAT material used in this work, Glass fibre: PPG2002, Epoxy: Prime 20 slow hardener

However, it is concluded from the verification that the results are highly influenced by stress concentrations, even with very small magnitudes. This is also evident when considering the small slope of the fatigue data.

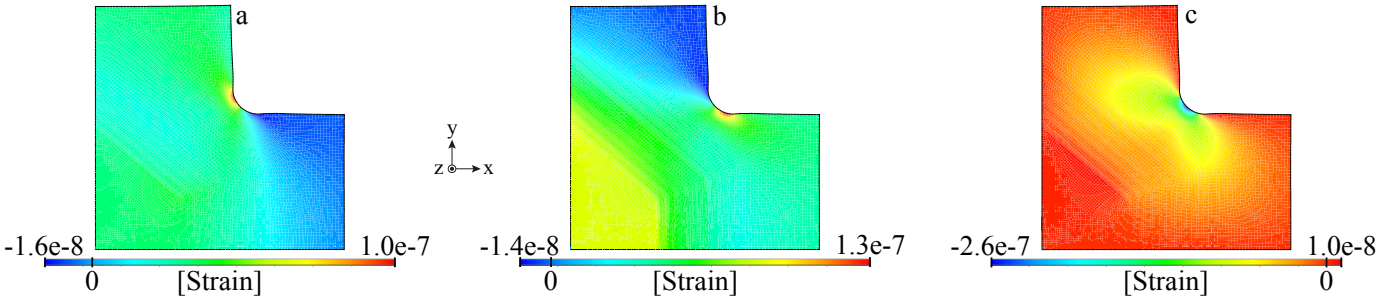

Fig. 2 Strains in the sub-structure in the Y-direction (a), the X-direction (b), and shear strain in the XY-plane (c) excluding the clamping areas

2.2 FE Model

ANSYS is used to conduct the FE analyses. The SHELL181 element, which is a 4-node element with 6 degrees of freedom, is used. Due to the geometric symmetry only a quarter of the sub-structure is modelled as shown in Fig. 1. Every ply-drop is modelled on element level in the FE model to obtain a model as close to the actual sub-structure as possible w.r.t. load introduction into the gauge zone and smoothness of the stiffness transitions. Displacement in the X-direction and rotation around the Y-axis are constrained at the vertical symmetry boundary and vice versa at the horizontal boundary. Furthermore, displacement in the Z-direction is constrained at both boundaries.

The loads are applied as evenly distributed forces at the ends of the arms. The strain distribution in the designed sub-structure is as shown in Fig. 2 with unity loads applied in the Y- and X-direction. In Fig. 2 it is shown that the strains are at a maximum in the corners which is not ideal, but as mentioned earlier the cruciform specimen design is the only applicable specimen type for this specific sub-structure. Nevertheless, the strains in the X- and Y-directions are high in the gauge zone, and the shear strain in the XY-plane is close to one order of magnitude lower in the gauge zone as well. This means that the desired strain ratio can be tested without disturbance from shear strains.

3. Fatigue Testing

Four fatigue tests are conducted on the test rig shown in Fig. 3 (a), however, the first two produce invalid results due to incorrect load introduction. Specifications for the test rig can be found in Laustsen et al. [16]. The specific loads applied for the two valid fatigue test are shown in Table 2. A static test is performed before the fatigue tests to help determine the required loads in both directions to achieve first failure in the sub-structure within 10^3-10^5 cycles.

The load in the Y-direction is applied in the bottom arm, while the top arm is constrained. Loads are applied in both arms in the X-direction to keep the centre of the sub-structure aligned with the load introduction in the Y-direction. Furthermore, the load in the X-direction is applied through spherical joints as shown in Fig. 3 (a). The spherical joints ensure that neither in-plane nor out-of-plane bending occurs, as long as only small displacements occur, and the load rods are aligned.

Data acquisition for strains, crack initiation, and crack propagation is obtained throughout testing via strain gauges, Digital Image Correlation (DIC) and a white light video camera for visual inspection. The strain gauges are positioned in the gauge zone to get a reference value for the strain. The DIC is used to obtain a full field measurement of the strains in the gauge zone to be compared to the strain field of the simulations. The DIC equipment is set up in a 3D configuration with two cameras to be able to compensate for out-of-plane movement. The video camera is used to track crack initiation and propagation, which can be done since the GFRP is transparent and cracks in the sub-structure change the refraction of the light. The placement of the measuring equipment w.r.t. the sub-structure is shown in Fig. 3 (b).

The sub-structure is loaded with a constant amplitude loading instead of a more realistic variable amplitude loading throughout the entire fatigue test. This is done because the material data from the OptiDAT database is based on constant amplitude loading. Therefore, testing the sub-structure in a constant amplitude loading as well, increases the similarities between the tests, which is important since the objective is to assess failure predictions with fatigue material data from a database and not different test methods. Furthermore, a variable amplitude increases the complexity of the test, and makes it more difficult to compare the test and the simulation.

As mentioned, the objective is to determine and characterize the

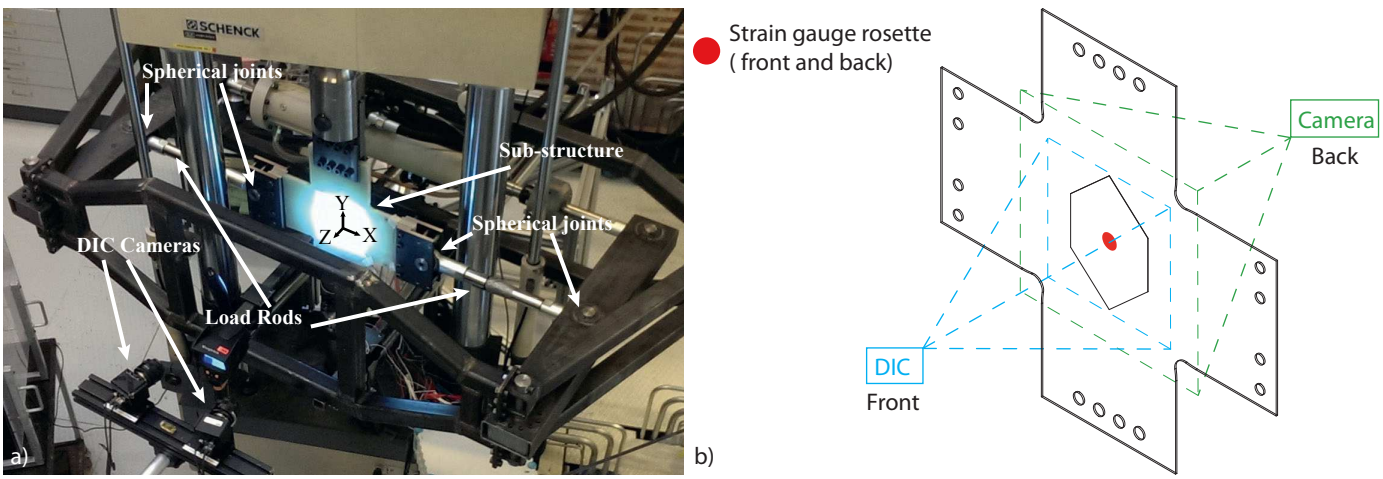

Fig. 3 The test rig used to conduct the fatigue testing (a), placement of the measuring equipment w.r.t. the sub-structure (b)

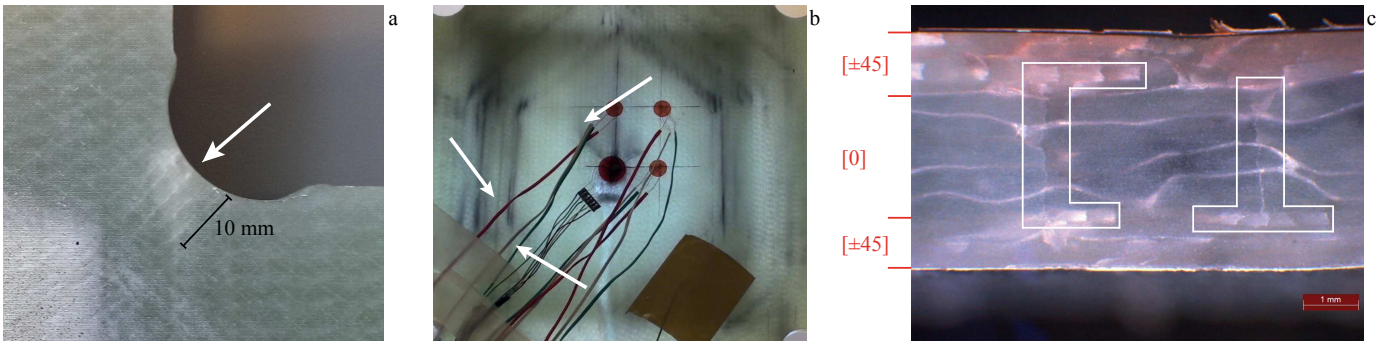

Fig. 4 Failures during testing, where (a) shows cracks in the corner in the top lamina and the $[0]$ laminae (fatigue test 1), (b) shows IFF cracks in the gauge zone (fatigue test 1), and (c) shows a microscopy image of IFF cracks in the gauge zone (static)

first failure in the gauge zone. It is estimated that the first failure is an IFF mode A parallel to the Y-direction in the $[0]$ lamina, based on the general observation that matrix cracks appear before any other cracks [21]. The IFF mode A is primarily initiated by tension loading transverse to the fibre direction and the fracture plane is perpendicular to this load direction. The IFF mode A and the other failure modes studied in this work are described in detail in [22]. The transverse strength of the UD GFRP lamina is the primary factor in estimating first failure. Therefore, it is possible to estimate a set of cyclic loads that can produce failure in the gauge zone within the predetermined number of cycles. This is done by considering the difference in static transverse strength between the material of the sub-structure, and the material from the database. This difference is used to parallel transport the S-N curve along the y-axis of the coordinate system to compensate for the difference.

3.1 Fatigue Test Results

The sub-structures used in the fatigue tests are quite complex, which means that the risk of manufacturing defects and hereby scatter between the sub-structures is high. For this reason only two of the four tested sub-structures produced usable data. Of the two tests that produced valid data, only during fatigue test 3 did IFF occur in the gauge zone, while in fatigue test 4 unintended IFF occurred in the ply-drops at the gauge zone.

The immediate damage during the static and fatigue tests are localized at the corners as expected as well as in the gauge zone (for the static test and fatigue test 3), shown in Fig. 4 (a) and (b), respectively. The damages in the corners include IFF cracks in the top ± 45 lamina at an angle of 45° that appeared late in the test, and IFF cracks in the $[0]$ laminae with increasing crack density throughout the test, as shown in Fig. 4 (a).

The fatigue tests were performed with a cyclic load ratio of $R = 0.1$ on the test rig as shown in Table 2. This resulted in crack initiations in and around the gauge zone as shown in Table 3. The load levels used in fatigue test 3 and 4 are chosen to obtain the same strain level and ratio in the centre of the gauge zone. The results are compared to the simulation results in section 4.

As desired, the cracks from the corners never entered the gauge zone during fatigue testing. However, due to the cracks in the fillet corners the strain in the gauge zone increased throughout the tests.

		Fatigue Test 3 [kN]	Fatigue Test 4 [kN]
Y-direction	Max Load	150	148
	Min Load	15	14.8
X-direction	Max Load	66.8	67.3
	Min Load	6.68	6.73

Table 2 Loads applied during each fatigue test.

	Fatigue Test 3			Fatigue Test 4	
Cycles	32000	93500	104000	17000	73000
Failure Position	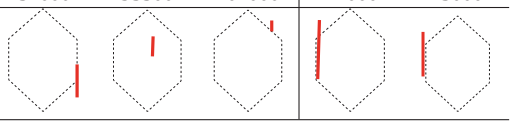				

Table 3 The dotted lines indicate the gauge zone and the red lines indicate failure.

The strain in the X-direction increased more than in the Y-direction because of the higher compliance in the X-direction due to the fibre orientation of the $[0]$-laminae. The increase in strain in the centre of the gauge zone throughout fatigue test 3 is shown in Fig. 5. Several crack initiations occurred in the gauge zone during testing as shown in Fig. 4 (b). Most of the cracks initiated close to the boundaries of the gauge zone and propagated through the gauge zone. These cracks are not initially delaminations but IFF cracks in the $[0]$ lamina, as shown in Fig. 4 (c). The figure also shows that when the IFF cracks in the $[0]$ lamina have propagated to the interface of the $[\pm 45]$ lamina the cracks make a 90° turn and propagate as delaminations in the $[0]$ and $[\pm 45]$ interface. Similar observations were done in [21].

4. Fatigue Simulation

The linear Fatigue Damage Simulator (FADAS) [15] is used to simulate the damage propagation in the corners of the modelled sub-structure to obtain the stiffness reduction associated with the damage in the corners. The FADAS algorithm is implemented into the commercial FE software ANSYS through a user material subroutine. By doing this the user material subroutine is called at every material integration point in the FE model at every equilibrium iteration in every substep in the Newton-Raphson solver. ANSYS passes stress and strain as input to the user material subroutine at the beginning of a substep, and the user material subroutine calculates the stress at the end of the substep [23]. The FADAS algorithm compares the calculated stresses to the residual strength of the material and degrades the stiffness if failure has occurred. This is shown as a flow chart in [15], and the algorithm is implemented as shown in the flowchart, except in this work the rainflow counting and cyclic stiffness degradation is not included. The rainflow counting is not included because a constant amplitude loading is applied. The cyclic stiffness degradation is not included because the focus of this work is to predict fatigue behaviour with a rather simple and fast model in order to minimise computational time in the design phase of large structures such as wind turbine blades.

In Puck's failure criterion a parameter η is introduced to account for degradation of stiffness after failure has initiated in an element, where the material degradation law in [15,22] is used in this

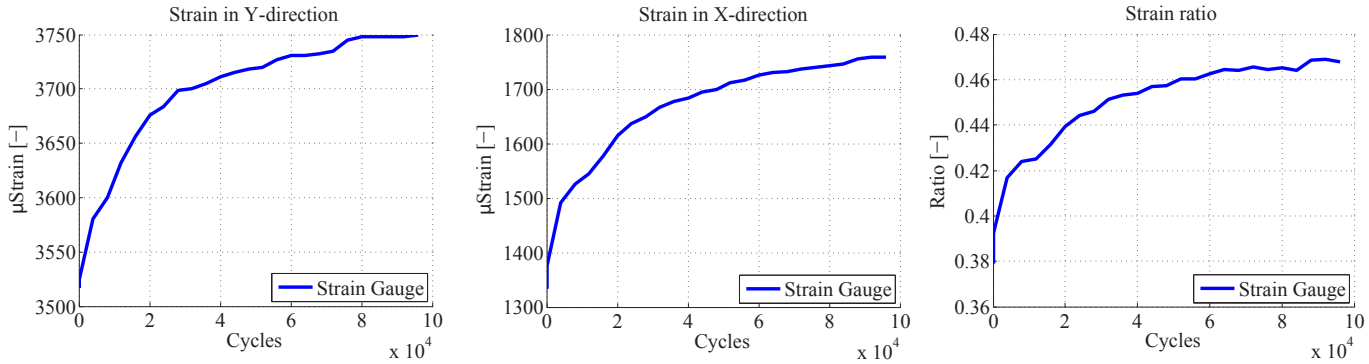

Fig. 5 Strain in Y and X-direction during fatigue testing

work. S-N data combined with a Constant Life Diagram (CLD) is implemented in the FADAS algorithm to determine damage based on applied stress from any given cyclic load ratio i.e. any mean stress. Furthermore, the Palmgren-Miner rule is implemented in a residual strength routine to accumulate damage due to shear and also due to tension and compression loads in the fibre and transverse direction, respectively.

A cycle jump routine is implemented to facilitate high-cycle simulations by simulating load cycles with a given interval [24]. Using a cycle jump approach may introduce inaccuracies in the prediction of damage and thus the local load redistribution after damage within the structure. In the test and simulation there is, only in the corners, a non-trivial progressive degradation of stiffness due to different types of failure, which is predicted by the FADAS algorithm. The goal of the simulations is to determine first failure based on global load redistribution. Therefore, local load redistribution in the corners does not have a big influence.

4.1 Simulation of the Sub-structure

A simulation of fatigue test 3 was performed with the same magnitude of loads applied as in the actual test. This resulted in a noticeable difference in strains measured by the strain gauge in the centre of the gauge zone and the calculated strains from the FEA. There are several possible reasons for this. One is that there is a difference between the stiffness of the material in the test and the simulation e.g. due to varying fibre volume fractions. Another possible reason is a change in load path between the simulation and the test, caused by either manufacturing defects, e.g. imperfect infusion of the fibres; air pockets; or resin rich areas, or imperfections in the geometry. These geometric imperfections include unevenly cut or placed fibre mats resulting in asymmetric ply-drops, or inaccurate cutting of the outer edges, leading to non-parallel edges or non-equal widths of the arms.

To compensate for the difference in strain in the gauge zone, a second simulation was conducted where the applied loads were calibrated to ensure similar strain levels in the gauge zone of the test and simulation. This was done because failure initiation is determined by the local strain level and not by the globally applied loads. To ensure similar strain levels, the loads are calibrated to approximately 133 kN and 63.6 kN in the Y- and X-direction in the simulation, respectively, compared to 150 kN and 66.8 kN in the test. The cycles for first failure along with the strain in the centre of the gauge zone at the first cycle are shown in Table 4. Since the simulation is based on an ideal model, and the actual sub-structure includes manufacturing defects, the failures will most likely initiate at different locations. Therefore, it makes no sense to determine first failure based on similar crack length in the simulation and test. Instead it is determined that first failure in the simulation is defined as the first cycle where three or more elements are exhibiting an IFF mode A failure in the gauge zone as shown in Fig. 6.

In the simulation, the cracks are initiated due to stress concentrations as it is shown in Fig. 6, where failure is initiated at the fillet corner and in the gauge zone. In the test, close to the gauge zone, most of the cracks initiate at other locations than in the simulation. There are three possible reasons for this. Either there are defects in these specific locations causing stress concentrations, or geometric imperfections are causing the stress concentrations to be shifted w.r.t. the simulation, or there are some 3D-effects not captured by the FE-model causing stress concentrations, or a combination of the three.

Result Type	Test	Load Calibrating	Strain Calibrating
Cycles	32000	10725 (66%)	24200 (24%)
$\epsilon_x[\mu strain]$	1355	1536 (13%)	1355 (0%)
$\epsilon_y[\mu strain]$	3507	3750 (7%)	3507 (0%)

Table 4 Cycles to first failure in the gauge zone, in the test and FADAS simulation. (The parentheses indicate deviation w.r.t the test result.)

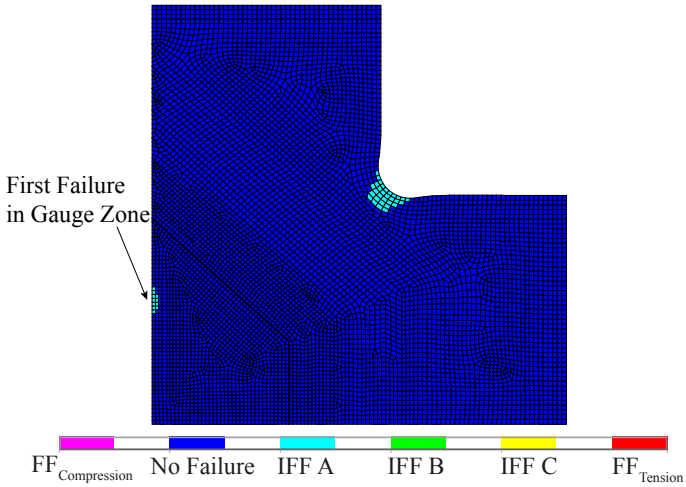

Fig. 6 Simulated first failure in the [0]-ply in the gauge zone

4.2 Comparison of results

The results from the simulation, DIC, and strain gauge measurements from the test are compared in Fig. 7. The results from the DIC equipment are obtained as an averaged value over the area where the strain gauge is attached, but the results are still affected by noise with a magnitude of $\pm 100\mu$Strain. As it is shown in Fig. 7 the results from the DIC in the Y-direction vary within the noise margin. Therefore, it is not possible to compare the DIC results in

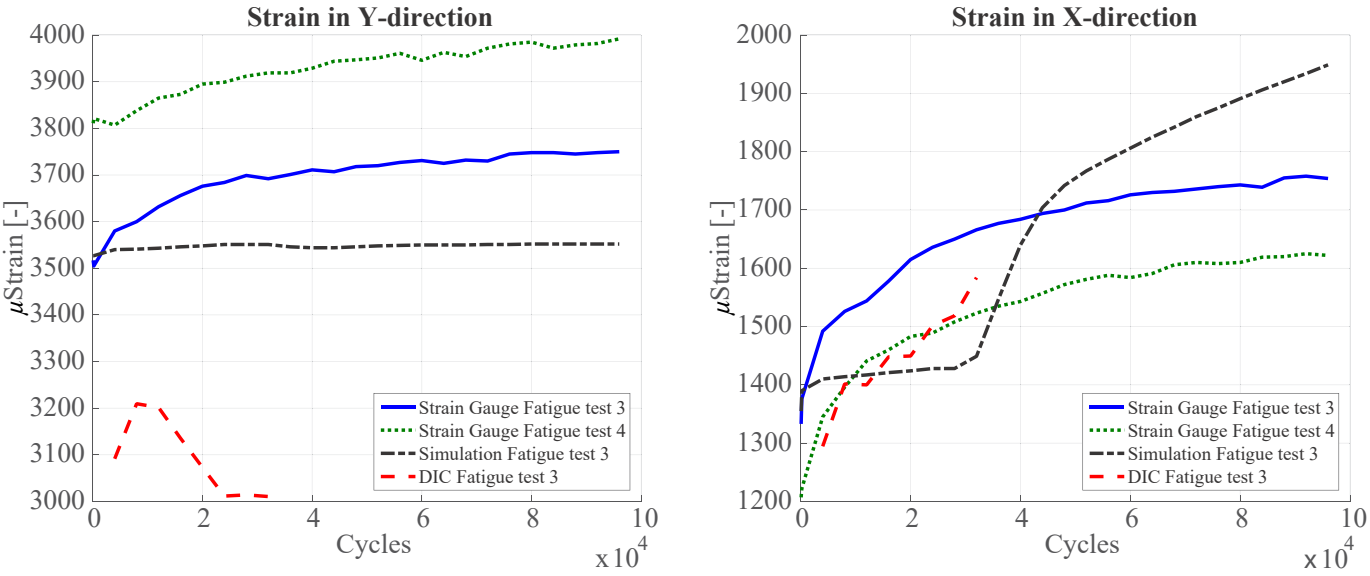

Fig. 7 Comparison of strains in simulation and test (No data was recorded using the DIC equipment after 32000 cycles)

the Y-direction with the results from the simulation and strain gauge. The DIC results in the X-direction show a similar tendency as the strain gauge results within the available accuracy.

The strain gauge results show that the strain in the centre region increases steadily throughout the test due to cracks elsewhere that lead to increased load transfer through the gauge zone.

The simulation results on the other hand, especially in the X-direction exhibit another behaviour. The strain in the centre of the gauge zone is constant in the Y-direction throughout the simulation. However, in the X-direction the strain increases slightly until 32000 cycles where the IFF mode A failure shown in Fig. 6 has propagated to the centre of the gauge zone where the strain value is extracted. The strain increases more rapidly after this, until IFF mode A failure is predicted just outside the gauge zone at 44000 cycles where the slope of the strain increment decreases due to load redistributions through the sub-structure. The results in Fig. 7 can also be interpreted as a mismatch between the stiffness degradation in the simulation and the test which leads to the important conclusion that a more accurate stiffness degradation model should be developed for the simulation model.

In Fig. 8 the deviation among the strain gauge results and the DIC and simulation results is shown throughout the test. The strain gauge results are used as reference because it is assessed that these results are most accurate. The deviation is less than 15% at all times. A 15% deviation has a huge effect on the fatigue life, since the fatigue life is very dependent on the strain level. One of the reasons for the deviation is that failures initiate at some locations in the sub-structure test, and are predicted at other locations in the simulation. This influences the results greatly because the strain is extracted as a point value, thus depending on the location of the damage the strain evolution at the data extraction point can vary.

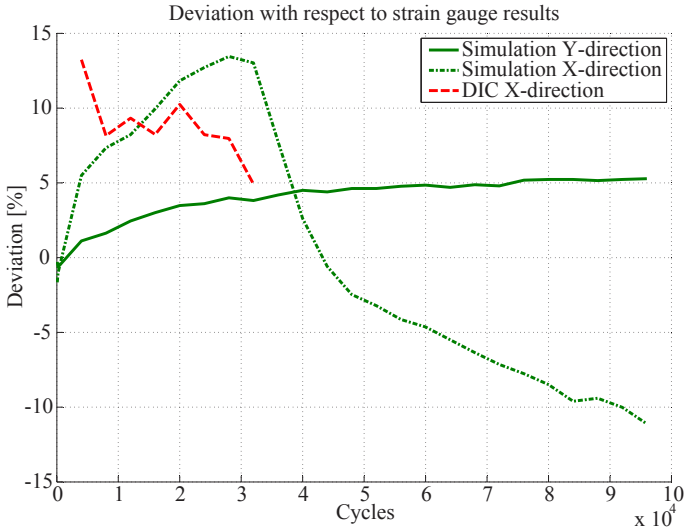

Fig. 8 The DIC and simulation results compared to the strain gauge results in fatigue test 3, respectively

5. Discussion

One of the general complications in this work is that the damages do not occur in the same locations in the simulation and the test. As mentioned, one of the reasons could be geometric imperfections causing stress concentrations to appear in other locations than in the ideal model. Fig. 9 (a) shows one of the sub-structures cut along the x-axis to obtain a closer look at the ply-drop geometry. It is clear that the sub-structure is not symmetric in the thickness direction. In particular, there is a rather large shift of the neutral axis indicated at (1). To test the effect of the shift of neutral axis, this asymmetry is introduced in the FE model as shown in Fig. 9 (b).

The considered asymmetric lay-up can be manufactured if one ply (yellow) on either side of the neutral axis is placed inaccurately and another (red) is cut inaccurately causing it to start further from the gauge zone as in the top right hand side of the asymmetric lay-up in Fig. 9 (b). It should be noted that the distance from one ply-drop to the next is 6.5 mm for the five ply-drops closest to the gauge zone, so it is very likely that the inaccurate ply placement described could occur in all of the sub-structures.

The neutral axis is not moved for the ply-drop closest to the gauge zone of the right hand side of the asymmetric lay-up because the added plies have the same stiffness as the middle plies, i.e. it corresponds to adding one ply on either side of the middle $[0_5]$-plies. The lay-up is modelled with the same lower geometry as a symmetric lay-up to simulate the sub-structure being positioned in a mould. The upper geometry is then the consequence of the inaccurately placed plies.

The stress in the x-direction, which is the primary cause of IFF mode A in this sub-structure, is shown for the symmetric and asymmetric

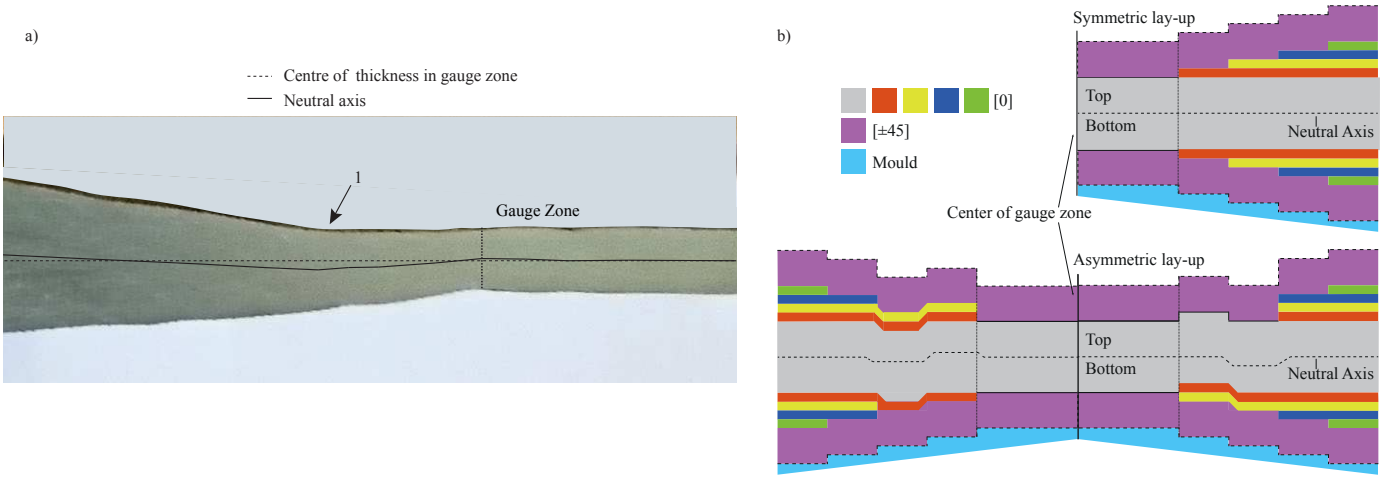

Fig. 9 Picture of the cross section of the gauge zone and ply-drops of a tested sub-structure (a), and asymmetric lay-up and neutral axis location in the model (b)

lay-up in Fig. 10. The highest stress in the x-direction is moved from the centre of the gauge zone to the ply-drop as shown in Fig. 10. This means that first failure will initiate from here in the simulation, which is also the case for the test. Hereby demonstrating that the location of the first failure event in the uniform strain field at the gauge zone is very sensitive to imperfections and stress raisers. Furthermore, making it plausible that a geometric imperfection is at least part of the reason for the failures not occurring in the same locations for the tests and simulation.

6. Conclusion

The internal ply-drops ensured that delaminations did not occur in the ply-drops as opposed to a milled gauge zone, but crack initiation still occurred in the ply-drops due to manufacturing defects and stress raisers possibly caused by the inaccurately placed plies as mentioned in section 5. The misaligned plies caused local out-of-plane bending resulting in higher local stresses. The plies were moved less than 13 mm, which entailed that the first failure initiation occurred at the ply-drop and not in the centre of the gauge zone.

Through this work it is concluded that results obtained from the test of the sub-structure are highly influenced by the accuracy of the manufacturing and lay-up process. However, manufacturing defects cannot be completely avoided in relatively complex structures such as the sub-structure used in this work. This leads to the conclusion that sub-structures should be designed in such a way that they are not particularly affected by manufacturing defects in order to obtain reliable results.

It is difficult to conclude if the inaccuracies in the fatigue predictions were due to the fact that the sub-structures were affected by the manufacturing defects, or if the material properties were too inaccurate. Nevertheless, Fig. 7 shows that the stiffness degradation trend predicted by the FADAS algorithm due to damage propagation is far from the trend measured in the test. It is the authors perception that this mismatch in stiffness trend is not caused by the fatigue material data, but rather the stiffness degradation model, which makes the evolution of damage predicted by FADAS questionable.

Acknowledgement

The authors acknowledges N. B. Grishauge and S. V. Pedersen for assistance with experiments and insightful input regarding the FE analyses.

References

[1] M. Quaresimin and P. A. Carraro, “On the investigation of the biaxial fatigue behaviour of unidirectional composites,” *Composites Part B:*

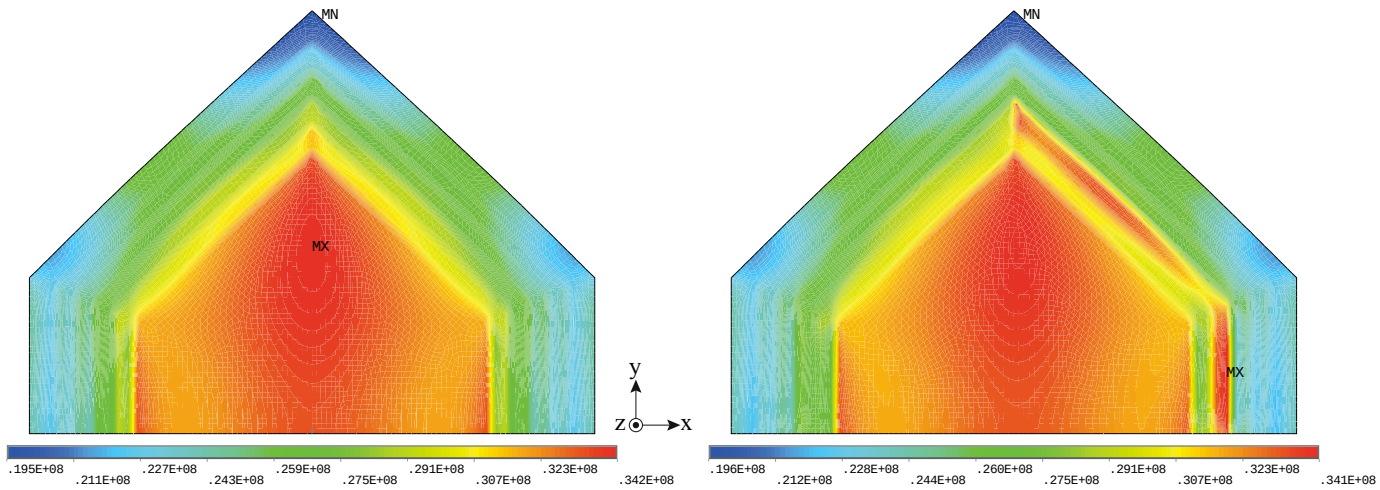

Fig. 10 Stress in the x-direction in the middle ply for the symmetric and asymmetric lay-up (Only the gauge zone and the five innermost ply-drops are shown)

Engineering, vol. 54, pp. 200–208, nov 2013. [Online]. Available: http://www.sciencedirect.com/science/article/pii/S1359836813002576

[2] D. Qi and G. Cheng, "Fatigue behavior of filament-wound glass fiber reinforced epoxy composite tubes under tension/torsion biaxial loading," *Polymer Composites*, vol. 28, no. 1, pp. 116–123, feb 2007. [Online]. Available: http://doi.wiley.com/10.1002/pc.20275

[3] S. Adden and P. Horst, "Damage propagation in non-crimp fabrics under bi-axial static and fatigue loading," *Composites Science and Technology*, vol. 66, no. 5, pp. 626–633, may 2006. [Online]. Available: http://www.sciencedirect.com/science/article/pii/S0266353805003131

[4] C. Kensche, "Final Report on Tube Testing," OPTIMAT BLADES, Tech. Rep., 2006. [Online]. Available: www.wmc.eu/public_docs/10370_000.pdf

[5] W. Liu, P. D. Soden, and A. S. Kaddour, "Design of end plugs and specimen reinforcement for testing 55 glass/epoxy composite tubes under biaxial compression," *Computers and Structures*, vol. 83, no. 12-13, pp. 976–988, 2005.

[6] R. Olsson, "A survey of test methods for multiaxial and out-of-plane strength of composite laminates," *Composites Science and Technology*, vol. 71, no. 6, pp. 773–783, apr 2011. [Online]. Available: http://www.sciencedirect.com/science/article/pii/S0266353811000509

[7] E. Lamkanfi, W. Van Paepegem, and J. Degrieck, "Shape optimization of a cruciform geometry for biaxial testing of polymers," *Polymer Testing*, vol. 41, pp. 7–16, feb 2015. [Online]. Available: http://www.sciencedirect.com/science/article/pii/S0142941814002189

[8] X. Zhao, Z. C. Berwick, J. F. Krieger, H. Chen, S. Chambers, and G. S. Kassab, "Novel Design of Cruciform Specimens for Planar Biaxial Testing of Soft Materials," *Experimental Mechanics*, vol. 54, no. 3, pp. 343–356, sep 2014. [Online]. Available: http://link.springer.com/10.1007/s11340-013-9808-4

[9] A. S. Torres and A. K. Maji, "The development of a modified bi-axial composite test specimen," *Journal of Composite Materials*, vol. 47, no. 19, pp. 2385–2398, aug 2012. [Online]. Available: http://jcm.sagepub.com/content/47/19/2385

[10] M. C. Serna Moreno and J. J. López Cela, "Failure envelope under biaxial tensile loading for chopped glass-reinforced polyester composites," *Composites Science and Technology*, vol. 72, no. 1, pp. 91–96, dec 2011. [Online]. Available: http://www.sciencedirect.com/science/article/pii/S0266353811003629

[11] E. Lamkanfi, W. Van Paepegem, J. Degrieck, C. Ramault, A. Makris, and D. Van Hemelrijck, "Strain distribution in cruciform specimens subjected to biaxial loading conditions. Part 1: Two-dimensional versus three-dimensional finite element model," *Polymer Testing*, vol. 29, no. 1, pp. 7–13, 2010. [Online]. Available: http://dx.doi.org/10.1016/j.polymertesting.2009.08.009

[12] A. Makris, T. Vandenbergh, C. Ramault, D. Van Hemelrijck, E. Lamkanfi, and W. Van Paepegem, "Shape optimisation of a biaxially loaded cruciform specimen," *Polymer Testing*, vol. 29, no. 2, pp. 216–223, 2010. [Online]. Available: http://dx.doi.org/10.1016/j.polymertesting.2009.11.004

[13] A. Smits, D. Van Hemelrijck, T. P. Philippidis, and A. Cardon, "Design of a cruciform specimen for biaxial testing of fibre reinforced composite laminates," *Composites Science and Technology*, vol. 66, no. 7-8, pp. 964–975, jun 2006. [Online]. Available: http://www.sciencedirect.com/science/article/pii/S0266353805003064

[14] V. a. Passipoularidis and P. Brøndsted, *Fatigue Evaluation Algorithms: Review*, 2009, vol. 1740, no. November.

[15] V. A. Passipoularidis, T. P. Philippidis, and P. Brøndsted, "Fatigue life prediction in composites using progressive damage modelling under block and spectrum loading," *International Journal of Fatigue*, vol. 33, no. 2, pp. 132–144, feb 2011. [Online]. Available: http://www.sciencedirect.com/science/article/pii/S0142112310001659

[16] S. Laustsen, E. Lund, L. Kühlmeier, and O. T. Thomsen, "Development of a High-fidelity Experimental Substructure Test Rig for Grid-scored Sandwich Panels in Wind Turbine Blades," *Strain*, vol. 50, no. 2, pp. 111–131, apr 2014. [Online]. Available: http://www.scopus.com/inward/record.url?eid=2-s2.0-84896397252&partnerID=tZOtx3y1

[17] E. Lamkanfi, W. Van Paepegem, J. Degrieck, C. Ramault, A. Makris, and D. Van Hemelrijck, "Strain distribution in cruciform specimens subjected to biaxial loading conditions. Part 2: Influence of geometrical discontinuities," *Polymer Testing*, vol. 29, no. 1, pp. 132–138, feb 2010. [Online]. Available: http://www.sciencedirect.com/science/article/pii/S0142941809001731

[18] R. Nijssen, "Wind Turbine Materials Research Database," Tech. Rep., 2011. [Online]. Available: http://www.wmc.eu/optimatblades_optidat.php

[19] T. K. Jacobsen, "Material specification, Reference material (OPTIMAT) glass-epoxy material," UPWIND project, Tech. Rep., 2002. [Online]. Available: www.wmc.eu/public_docs/10004_001.pdf

[20] T. P. Philippidis, "Verified Material Model Incorporating Progression of Damage Due To Static Loading and the Effect of Fatigue on Residual Strength and Stiffness," *Project Upwind*, pp. 1–85, 2011.

[21] R. D. Jamison, K. Schulte, K. L. Reifsnider, and W. W. Stinchcomb, "Characterization and Analysis of Damage Mechanisms in Tension-Tension Fatigue of Graphite/Epoxy Laminates." *ASTM Special Technical Publication*, pp. 21–55, 1984. [Online]. Available: http://www.scopus.com/inward/record.url?eid=2-s2.0-0021598748&partnerID=tZOtx3

[22] A. Puck and H. Schürmann, "Failure analysis of FRP laminates by means of physically based phenomenological models," *Composites Science and Technology*, vol. 62, no. 12-13, pp. 1633–1662, 2002. [Online]. Available: http://www.sciencedirect.com/science/article/pii/S0266353801002081

[23] ANSYS, "ANSYS USER Material Subroutine USERMAT," Tech. Rep., 1999.

[24] E. N. Eliopoulos and T. P. Philippidis, "A progressive damage simulation algorithm for GFRP composites under cyclic loading. Part II: FE implementation and model validation," *Composites Science and Technology*, vol. 71, no. 5, pp. 750–757, 2011. [Online]. Available: http://dx.doi.org/10.1016/j.compscitech.2011.01.025